22

BioSonar: a Bio-Mimetic Approach to Sonar Systems Concepts and Applications

Yan Pailhas, Chris Capus, Keith Brown and Yvan Petillot
Heriot-Watt University, Ocean Systems Laboratory
Scotland, UK

1. Introduction

1.1 Traditional sonars

This chapter is a contribution to the underwater acoustic field. SONAR (SOund Navigation And Ranging) was invented and developed during the first world war based on observations of dolphins (in water) and bats (in air) of their capabilities to detect objects and navigate into a 3D world. Sonar systems have evolved dramatically since then from a simple ranging system to complex sonar imaging systems. Several configurations for underwater sonars are available (cf. figure 1) and the most popular are:

- profiler: the sonar is usually mounted vertically on a vehicle (boat, AUV...) and gives, as its name indicates, a 3D profile of the seabed or bathymetry.
- sidescan: sidescan sonars insonify perpendicularly to the trajectory of the vehicle (sideways). The port and starboard pings are stacked to form an image. They provide sonar images of the survey area.
- forward-looking: the sonar is pointing forward. The bearing angle is given thanks to a mechanical scan or electronic beam forming.

In recent years, manufacturers have come a long way in the imagery systems both in the sidescan and the forward-looking sonars focusing on providing very high resolution sonar images. The latest technology developed is the SAS system (Synthetic Aperture Sonar) which is based on the ideas from SAR (Synthetic Aperture Radar) technology. SAS systems provide sidescan-like images with a constant centimetric resolution over the whole range. In order to increase the sonar resolution and by doing so the overall quality of sonar images, manufacturers have chosen to increase the frequency. The resolution is linearly dependant on the wavelength λ ($\lambda = c/f$ where c is the sound speed in water and f the frequency). The final image is computed using only the amplitude of the signal. The main reason behind this is that we (humans) are more comfortable with an optic-like incoherent image. Sonar was inspired from dolphins and bats in its early stages, but now its practical engineering has evolved toward an imaging system.

1.2 Chapter structure

This chapter is organised as follows:
We analyse the dolphins' sonar in section 2. Dolphins use a large variety of clicks depending on the tasks they have to perform. We study the dolphins' behaviour click pattern, then the

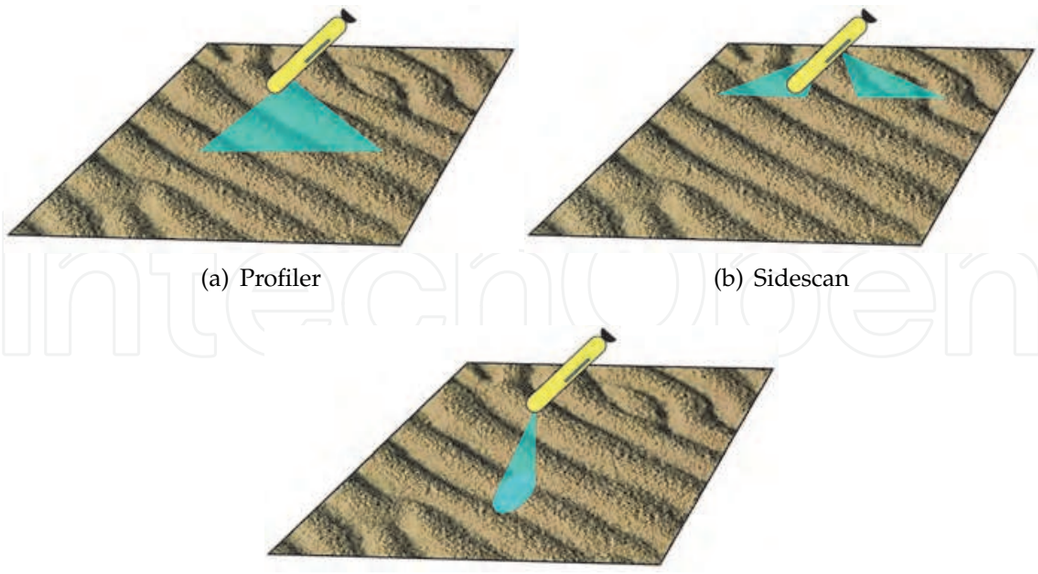

(a) Profiler (b) Sidescan

(c) Forward looking

Fig. 1. Classical sonar configurations: *(a)* profiler, *(b)* sidescan and *(c)* foward looking.

structure of the dolphins' click itself using the fractional Fourier transform. This analysis leads to a model for synthetic bio-mimetic pulses for a bio-sonar system. In section 3, we give our interpretation of a bio-mimetic sonar, the bio-sonar, using bio-mimetic pulses. We explain how to interpret the target echoes in section 4 and show how a target can be identified unambiguously. In section 4 we show two applications of the BioSonar and how it outperforms traditional sonar. In section 4.1 we describe how a bio-mimetic sonar can be used in the MCM (mine counter measure) context. Then in section 4.2 we show its performance in cable tracking.

2. Dolphin sonar

2.1 Dolphins' sonar capability

Dolphin sonar is the result of a million years of evolution. The dolphin echolocation systems are well known for their excellent performance and have been studied for decades Au (1993). They significantly outperform man-made sonars. They have shown excellent capabilities for object detection and identification, especially in complex environments such as very shallow water and cluttered locations. As an example, Moore et al. (1991) studied the capability of dolphins to identify the contains of aluminium flask bottle suspended in mid-water. The US navy have trained dolphins for complicated tasks such as mine detection and harbour inspection.

2.2 Analysis of real dolphin clicks

Based on observations of dolphins' echolocation clicks, Houser introduced in Houser et al. (1999) a taxonomy for the variety of clicks emitted based on their frequency content. The taxonomy is described in Table 1. This particular click taxonomy identified several click types based on distributions in two main spectral regions, one at low frequency (<70 kHz) and the other at higher frequency (<70 kHz).

A	unimodal, low frequency (<70 kHz)
B	unimodal, low frequency (<70 kHz); 2nd peak (>70 kHz) between -3 and -10 dB down
C	bimodal; low and high frequency peaks within -3 dB
D	unimodal, high frequency (>70 kHz)
E	unimodal, high frequency (>70 kHz); 2nd peak (<70 kHz) between -3 and -10 dB down
W	wideband; single continuous bounded region within -3 dB limit (freq. bandwidth >85 kHz)
M	multimodal; three or more distinctly bounded regions within -3 dB limit

Table 1. Click taxonomy from Houser et al. (1999)

In Martin et al. (2003) and Houser et al. (2005), the authors collect the echolocation clicks produced by dolphins while they are performing a bottom-object search experiments in San Diego Bay. Two dolphins were trained specifically for this experiment. The echolocation clicks and their corresponding echoes were recorded using instrumentation package, the biosonar measurement tool (BMT). The tool was carried by the dolphins.

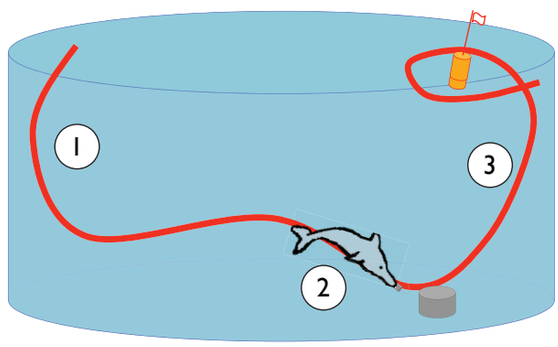

Fig. 2. Dolphin's behaviour during the free-swimming experiment. **(1)** detection and localisation of the target, **(2)** target identification and **(3)** return to the boat.

Figure 2 shows a sketch of the dolphin's behaviour during the free-swimming experiment. During phases 1 and 3, the dolphin is respectively searching for the target on the seafloor and the boat at the surface. The clicks emitted during these detection phases are typically low frequency (predominantly type A). When the dolphin finds the target (phase 2), it starts an interrogation strategy, *pinging* the target more frequently. The variety of clicks used during the interrogation is much larger than during the other phases, and the click pattern contains all of the click types described by Houser in the taxonomy.
Dolphins echolocation clicks are very short impulsive sounds. A typical click duration is around 80 μs Au (1993). For this reason, related to the uncertainty principle Cohen (1995), classical time frequency representations such as the spectrogram or Wigner-Ville distribution struggle to extract meaningful structure within the pulse without *prior* knowledge.
In Capus & Brown (2003) and Bultan (1999), the authors studied the echolocation clicks of the big brown bat (*Eptesicus fuscus*). Time-frequency analyses indicated that these signals are made up of three or four distinct downchirp components. By analogy we look for downchirps in the dolphin clicks. Linearisation of the problem leads to the emphasis of linear downchirp

components in the dolphin clicks. This can be achieved by computing the fractional Fourier transform (FrFT) of the signal. The fractional Fourier transform of a function $f(x)$ is given by Eq. 1

$$F^{\alpha} f(x) = \frac{\exp\left(-j\left(\frac{1}{4}\pi\hat{\phi} - \frac{1}{2}\phi\right)\right)}{2\pi|\sin\phi|^{1/2}} \exp\left(\frac{1}{2}jy^2\cot\phi\right) \times \int_{-\infty}^{+\infty} \exp\left(-\frac{jxy}{\sin\phi} + \frac{1}{2}jx^2\cot\phi\right) f(x)\mathrm{d}x \tag{1}$$

where $\alpha \in [0,\ 1]$ represents the transform order, $\phi = \alpha(\pi/2)$ and $\hat{\phi} = \mathrm{sgn}(\phi)$.
Figure 3(a) displays the time representation of a type B dolphin click. In figure 3(b) the power spectra of the same click are computed using the classical Fourier transform and the fractional Fourier transform.

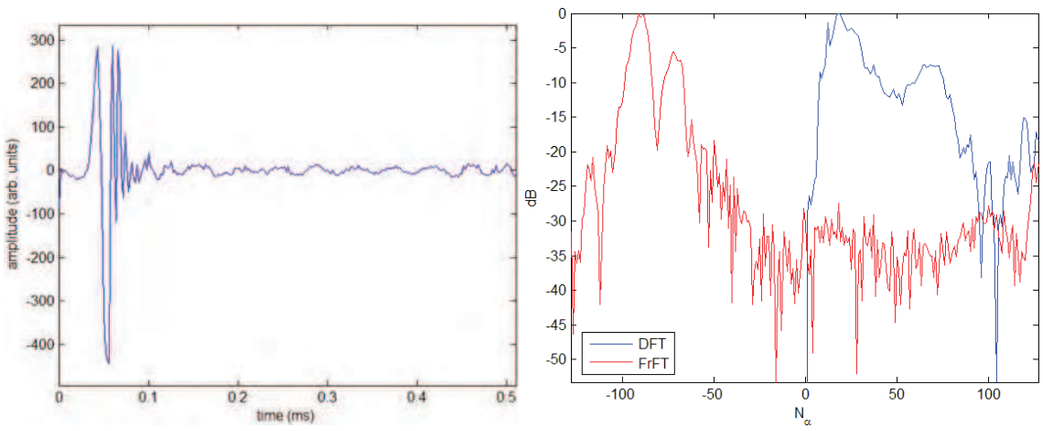

(a) Time domain (b) Fourier and Fr. Fourier domain

Fig. 3. Representation of a type B dolphin click in (a) the time domain and (b) Fourier and Fractional Fourier domain.

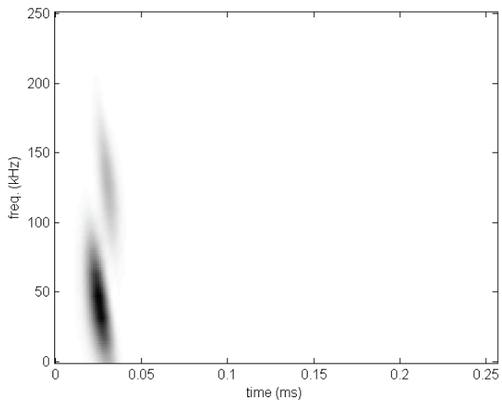

Fig. 4. Time-frequency representation of the type B dolphin click from Fig. 3 using the squared modulus of the short-time fractional Fourier transform.

The two concentrations of energy in the FrFT representation of the type B click in figure 3(b) confirm the presence of two chirp components. Figure 4 displays a short-time FrFT of the same signal. A double downchirp structure is clearly visible here.

3. BioSonar principles

So what makes dolphins' sonars so efficient? The short answer lies in the fact that they have a brain directly linked to their sonar system and are able to analyse directly the echoes. But one can argue that sonar experts struggle to find their objects of interest in a very cluttered environment even by analysing very high resolution images such as SAS images. Two elements of response to this question are given by analysing the dolphins' behaviour (especially their click pattern when they perform identification tasks) and the simplifications of man-made sonar systems:

- Complex broadband clicks: conventional sonars use narrowband out-going pulses. Dolphins are using a variety of broadband clicks and studies show that the diversity of clicks is adapted to the current task and environment.
- Fine echo analysis (the forgotten phase): in the classical sonar processing, we highlighted the fact that only the amplitude of the signal is usually used for the image processing. By doing so a tremendous quantity of information is rejected.

In this section we describe our bio-mimetic sonar system. The aim of our approach is to resolve the points previously highlighted:

- Biomimetic dolphin-like signals are built based on the analysis of real dolphins' clicks. We will show that we can reconstruct the whole click variety of the dolphins' clicks taxonomy.
- A fine echo analysis is proposed in order to take into account the forgotten phase of the signal. In particular we will show that any object has characteristic acoustic resonances, which can be extracted and used as features for classification / identification.

3.1 Biomimetic pulses

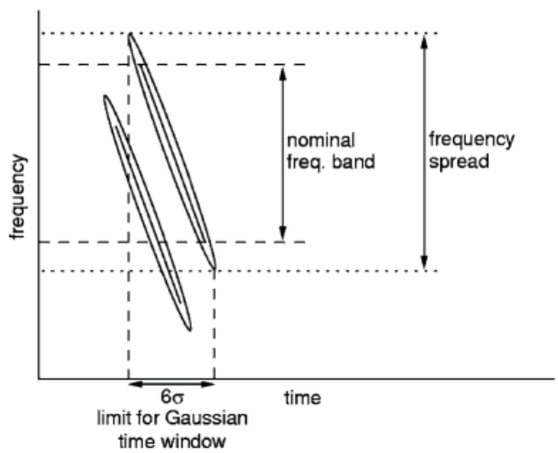

Fig. 5. Time-frequency representation of the bio-inspired double chirp signals.

In Capus et al. (2007), Capus et al. proposed a model for bio-inspired pulses based on the observations made in section 2.2. The bio-mimetic pulses copy the double downchirp

structure highlighted in figure 4. Figure 5 displays the chirp components for the bio-inspired double chirp signals. The bio-mimetic pulses are around 50% longer than natural dolphin signals, with a time duration of 120 μs. The pulses cover a similar bandwidth to natural dolphin clicks (30 - 130 kHz). Each individual chirp has a duration of 100 μs and the two downchirp components are separated by 20 μs. This particularity follows the analyses from real dolphin clicks: the higher frequency chirp is always delayed relative to the lower frequency one.
In total a series of six bio-mimetic pulses have been created and named DCn with $n \in [1, 6]$. Table 2 describes the nominal frequency and the chirp rate for the two donwchirps for all the DCn pulses. Note that each individual downchirp are weighted using a 6 σ gaussian window.

signal	Chirp rate (kHz.s^{-1})	Chirp 1	Chirp 2
DC1	-0.420 $\times 10^6$	30 - 114 kHz	46 - 130 kHz
DC2	-0.375 $\times 10^6$	30 - 105 kHz	55 - 130 kHz
DC3	-0.330 $\times 10^6$	30 - 96 kHz	64 - 130 kHz
DC4	-0.300 $\times 10^6$	30 - 90 kHz	70 - 130 kHz
DC5	-0.270 $\times 10^6$	30 - 84 kHz	76 - 130 kHz
DC6	-0.240 $\times 10^6$	30 - 78 kHz	82 - 130 kHz

Table 2. Set of the DCn pulses.

Figure 6 displays an example of three bio-mimetic signals, DC1, DC3 and DC6, in the time domain and in the frequency domain. DC1 can be identified as a unimodal high frequency with a second peak in the lower frequency . DC3 is a multimodal with three distinctly bounded regions. And DC6 is bimodal, low and high frequency with -3 dB.

3.2 Object identification via broadband echoes

At first active sonars were used as a range measurement tool. By measuring the time t between when the system send the pulse and when the echo arrives, and knowing the sound speed c in water, one can compute the range r between the sonar and the target by the simple equation: $r = ct/2$.
However the understanding of the full echo structure requires the resolution of the wave propagation equation (Eq. 2). The main equation to solve is then the wave propagation equation of the displacement $\vec{u}$. It can written as follows:

$$(\lambda + 2\mu)\vec{\nabla}.\vec{\nabla}.\vec{u} - 2\mu\vec{\nabla} \times \vec{\nabla} \times \vec{u} = \rho\frac{\partial^2\vec{u}}{\partial t^2} \tag{2}$$

λ and μ represent the Lamé parameters, ρ the material density.
Note that for a fluid the displacement $\vec{u}$ is linked to the pressure p through the following equation:

$$\vec{u} = -\frac{\vec{\nabla}p}{\omega^2\rho} \tag{3}$$

where $\omega = 2\pi f$ represents the angular frequency.
This partial differential equation has been solved for simple cases such as spheres, cylinders (Faran (1951); Hickling (1962)), spherical shells in Goodman & Stern (1962) and cylindrical shells in Doolittle & Uberall (1966). Analytical solutions are not available for objects with more complex shape, and numerical simulations or models are needed at this point.

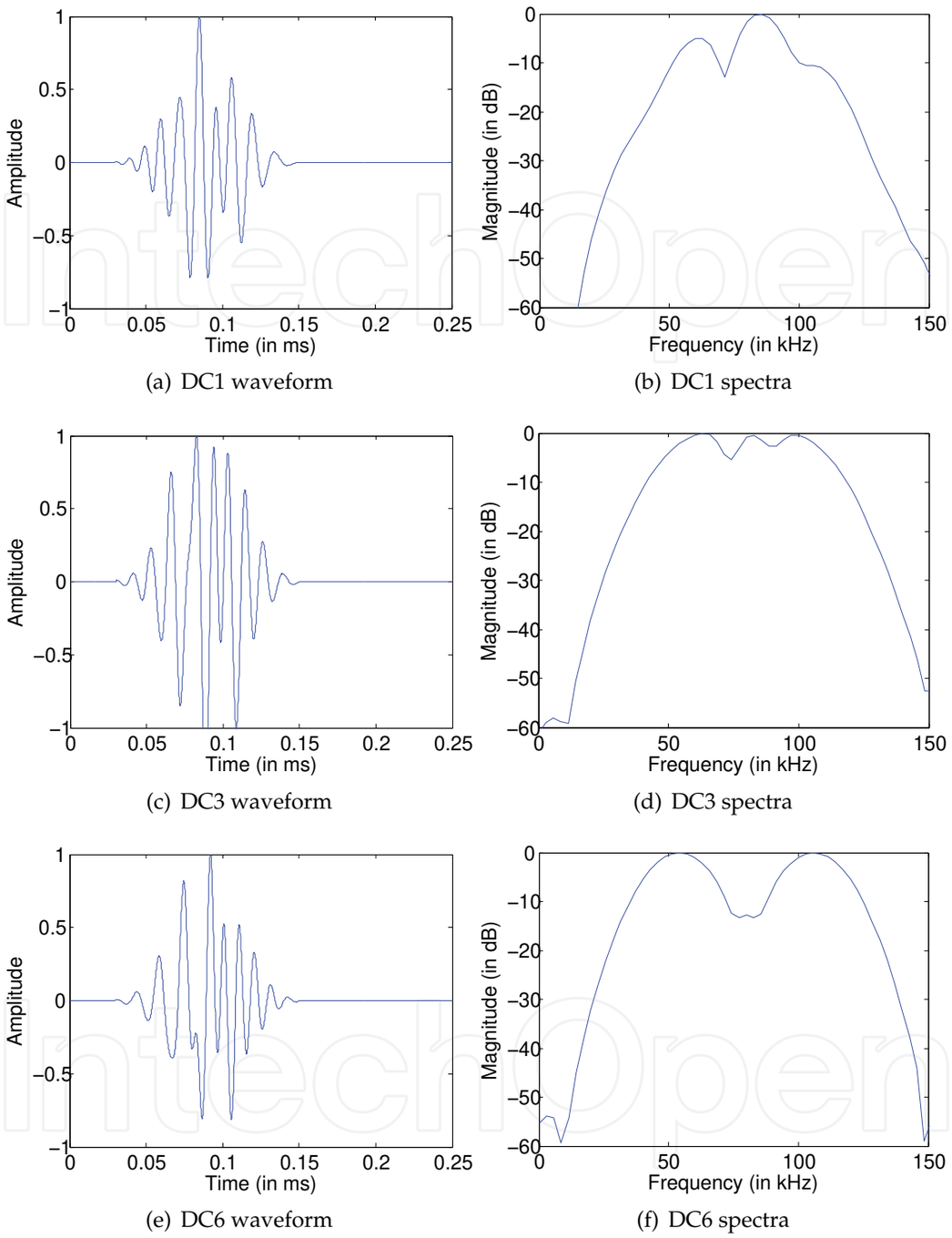

(a) DC1 waveform (b) DC1 spectra

(c) DC3 waveform (d) DC3 spectra

(e) DC6 waveform (f) DC6 spectra

Fig. 6. Examples of three bio-mimetic signals: DC1, DC3 and DC6.

The echo is the result of the interaction of the incoming acoustic wave with the target of interest. Echoes are characterised by multiple returns from the target. In the Fourier domain these multiple returns interfere and create notches in the echo spectra. Pailhas et al. (2010) proved that the localisation of the notches are stable features for identification. The feature

extraction can be computed as followed:

Let F be the spectrum of the backscattered echo and let $\{\omega_n\}_{n\in[1,\,N]}$ be the location in frequency of the notches. We associate ΔF to F by:

$$\Delta F(\omega) = \sum_{n=1}^{N} \delta(\omega - \omega_n) * G_\sigma(\omega) \tag{4}$$

where δ represents the Dirac function and G_σ is the centered Gauss function with a variance of σ. The ΔF function is an irregular Gauss comb where the peaks represent the notch locations. A metric can be associated to this space, and the distance between two elements ΔF and ΔG can be defined by:

$$d(\Delta F, \Delta G) = \left(\int_0^{+\infty} |\Delta F(\omega) - \Delta G(\omega)|^2 d\omega \right)^{1/2} \tag{5}$$

Classification using this distance metric has been tested in a controlled environment (Pailhas et al. (2010)). Six man-made targets of similar dimensions but different shapes and materials were used for this experiment. The correct identification rate was greater than 90%. Table 3 shows the confusion matrix of the broadband classifier using the distance defined by Eq. 5 and the two bio-mimetic pulses DC1 and DC6.

DC1 & DC6	cone	cone 8° tilted	pipe	tube	rocket head	brick (length)	brick (width)
cone	**0.50**	0.21	0	0	0	0	0
cone 8° tilted	0.29	**0.59**	0.05	0	0	0	0
pipe	0.12	0	**0.81**	0.06	0	0	0
tube	0.09	0.12	0	**0.94**	0	0	0
rocket head	0	0.08	0.14	0	**1.00**	0	0
brick (long)	0	0	0	0	0	**1.00**	0
brick (large)	0	0	0	0	0	0	**1.00**

Table 3. Confusion matrix for the fusion system of the two classifiers relative to the two bio-mimetic pulses DC1 and DC6.

The RST (resonance scattering theory) predicts strong interferences in the frequency range $ka \in [10,\ 50]$ where $k = \frac{2\pi f}{c}$ is the wavenumber, f the frequency, c the speed of sound in water and a is a key target dimension (e.g. radius for a cylinder or a sphere) Gaunaurd & Uberall (1983). This simply stipulates that the distance between two principal scatterers in the target should be larger that one wavelength to create measurable interferences and smaller than ten wavelengths for the interferences to be trackable.
Our transducers cover the same frequency band used by the dolphins: from 30 kHz to 130 kHz. According to the RST, this frequency band is optimal to characterise objects with a key target dimension included between 2 cm and 40 cm. We note that these dimensions match with the prey of dolphins.

4. Applications

In this section we discuss two applications of the BioSonar and how it outperforms traditional sonars. First we will describe how a bio-mimetic sonar can be used in the MCM (mine countermeasures) context. Then its performance in cable tracking application is shown.

4.1 Mine countermeasures

Detection, classification and identification of underwater objects continues to be a major issue for the military. Mine countermeasures were traditionally performed by dedicated ships and trained divers. With the technology pushing forward, MCM evolves toward a greater autonomy including autonomous vehicles and autonomous algorithms to detect and identify underwater mines. The traditional approach to ATR (autonomous target recognition) is image based. Extended research has been done on the subject. Calder et al. (1997); Goldman & Cohen (2004); Maussang et al. (2007) aim to detect global rarity in the sonar image using the assumption that a mine is a rare event. In Calder et al. (1998); Dobeck et al. (1997); Dura et al. (2002); Mignotte et al. (2000); Reed et al. (2003a;b) a model base approach is considered. Using simulations, a model of the expected target is created and compared to the detected object. Classical approaches using supervised learning have also been considered by Azimi-Sadjadi et al. (2001); Ciany & Huang (2000); Fawcett (2001); Perry & Guan (2001); Zerr et al. (2001).
Despite the high performances of the new generation of imagery sonars (including SAS systems), ATR using imagery is still at this stage unreliable due to a high false alarm rate and poor performances in heavily cluttered area (Petillot et al. (2010)). In parallel, the US Navy Mammal Program had trained dolphins from the 60's to detect and identify underwater mines. Dolphins' capabilities for manmade object detection suggest that useful information for MCM can be extracted from broadband echoes.
The background research described earlier led us to build an AUV (autonomous underwater vehicle) ready BioSonar which can be plugged directly on a REMUS-100 AUV. The BioSonar prototype has been mounted in a side-looking configuration to facilitate gathering of collocated sidescan data using the vehicle's standard Marinesonics sonar at 900 kHz operating frequency.
A series of trials have been done in Loch Earn (Scotland) in March 2010. The aim of these trials was to validate the capacity of the BioSonar for target recognition in a real environment operating from a reliable and commonly used autonomous vehicle. A set of spherical targets has been put together for these trials. Spheres provide a good reference target because of their rotational symmetries. The target itself will give a similar echo response at any angle of view, range or altitude. All the targets have a similar diameter (between 28 cm and 38 cm) and were made using different materials: stainless steel, concrete or plastic. Using conventional imagery sonar it is impossible to identify one target from another. Two experiments have been done in two different area of the loch:

- Area 1 is a relatively flat region (depth around 38 metres) giving good conditions for multi-aspect survey of the full target set.
- Area 2 lies on a steeper slope near the mouth of a river which drains into the loch.The river has brought a considerable quantity of debris into the loch consisting primarily of rocks and tree trunks and branches. Consequently, this area is heavily cluttered.

In Area 1 we aim to demonstrate the capability to distinguish targets with the same shape and similar dimensions but constructed from different materials or to distinguish a solid target from a hollow target. These are fundamental capabilities for the recognition of manmade targets amongst natural clutter objects. In Area 2 we aim to demonstrate the capability to reject clutter returns on the strength of their spectral content and lack of any consistent match or similarity with the echo responses of the manmade test targets. Rapid rejection of clutter contacts is another fundamental requirement for the effective recognition of manmade targets in a highly cluttered environment.

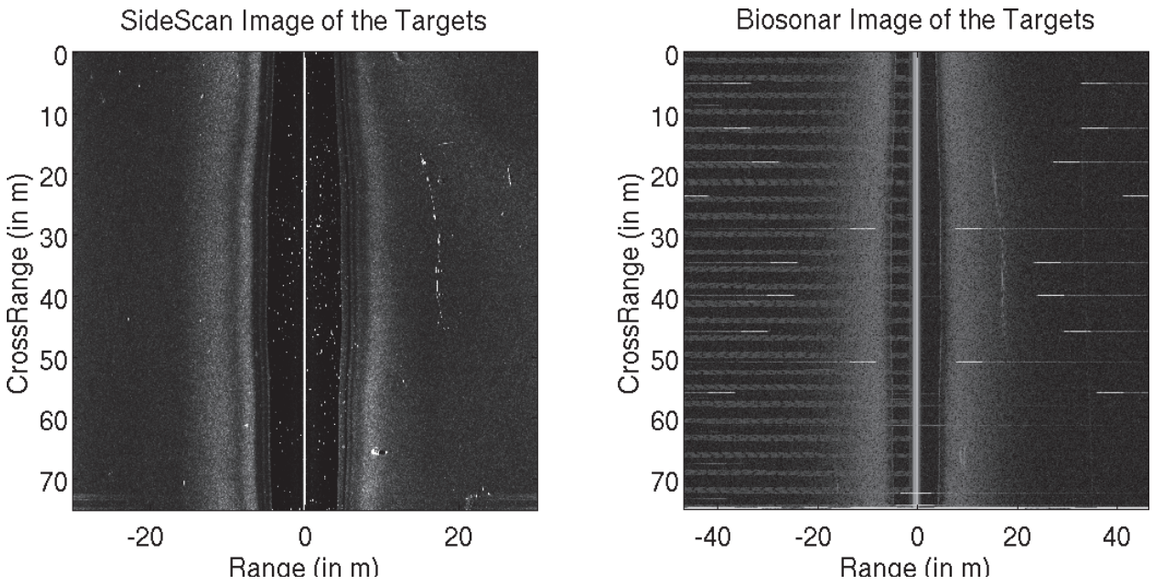

Fig. 7. Display of the sidescan sonar image of the targets (on the left), and the BioSonar image of the targets (on the right).

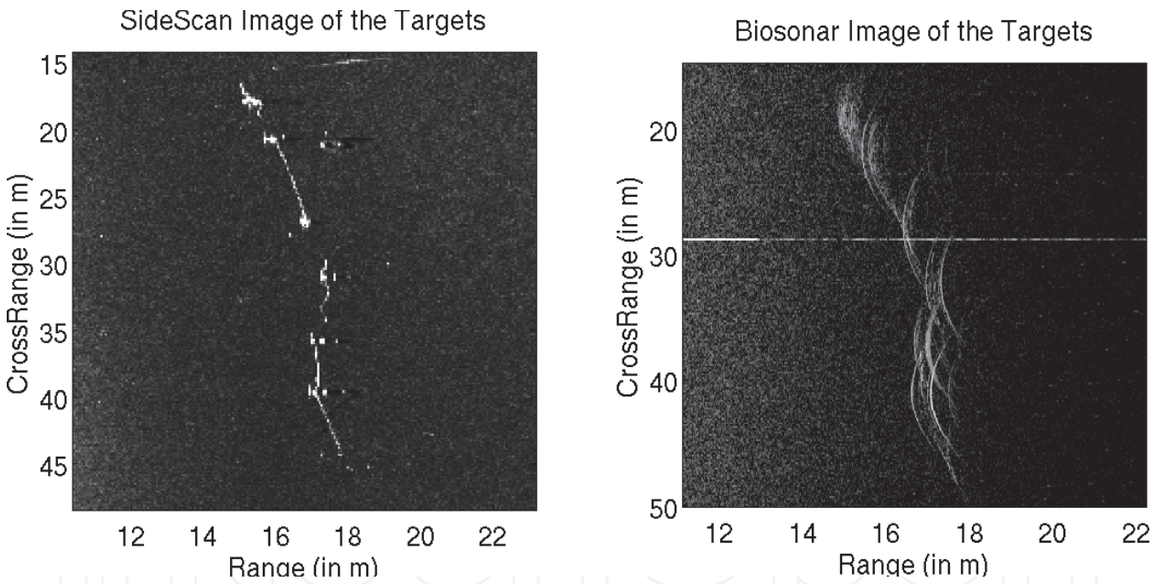

Fig. 8. Spherical targets with roughly the same dimension (Ø: around 30 cm) but built with different materials (plastic, aluminium or concrete) have been put on the seafloor. The figure displays a close up of the targets using sidescan (on the left), and using BioSonar (on the right). All the targets appear very similar in the sidescan image and are impossible to differentiate. However in the BioSonar image, the characteristic resonances of the different targets are clear which make the identification possible.

Figures 7 and 8 show one parallel path past the targets at around 16 metres range. The sidescan maximum range is fixed at 30m and the BioSonar system is running at approximately 46m maximum range. The registered sidescan image is displayed on the left, and the BioSonar

image on the right. The BioSonar images are produced for visualisation purposes only from the envelope of the matched filtered echo.
Figure 8 shows close ups over the target set for both sensors. Note that the wide beamwidth of the BioSonar system, leads to the target responses tracing arcs through the data, in similar fashion to raw SAS. The sidescan gives quite high resolution images allowing us to clearly locate each of the targets and gives a good response along the line connecting them (8mm braided polyethylene). Note that in the sidescan image, it is impossible to identify one target from another. Multiple responses at broadside do give some indication that certain targets are strongly resonant. Whilst precise location is more complicated working from the wideband returns, the resonances are more easily picked up in the parallel arcs associated with these targets.

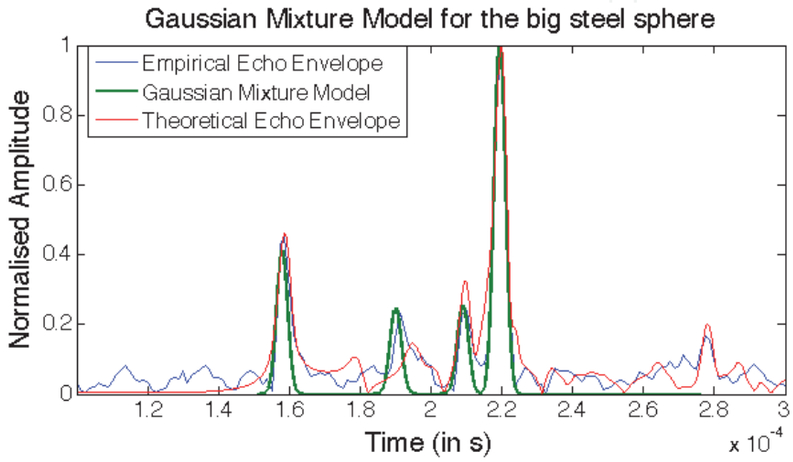

Fig. 9. Time-frequency representation of the bio-inspired double chirp signals.

In the following paragraphs we demonstrate an identification method using a time-domain Gaussian mixture model to represent the echo of the large steel sphere. Note that the time domain refers to the match filtered echo. A mixture of 4 gaussians has been chosen to model the envelope of the backscattering echo of the big steel sphere. The time domain methods suffer some limitations. In particular the match filtering in the time domain compresses the broadband pulses and tends to suppress the frequency dependance of single echo (especially the secondary echoes) and spread the envelope. However the bandwidth used by the BioSonar provides relatively clear echo and almost linear echo in the frequency domain. For this reason the resulting match filtered echo exhibits strong and sharp specular and secondary echoes for the targets of interest. Figure 9 displays a match between the empirical sphere echo and the gaussian mixture model.
Figure 10 shows positive identifications of the the steel sphere amongst the other targets at various ranges and orientations relative to the direction of deployment. The BioSonar image is given in the left column with the corresponding detection result on the right. In all cases the lower log-likelihood values indicate higher confidence in recognition. The resonant targets similar to the large steel sphere such as the small steel sphere or the PVC sphere are 10 dB higher in the log-likelihood feature and the background is 20 dB higher.
In figure 11, the algorithm has been run over the cluttered area (Area 2) with none of the prepared targets present. All the ATR algorithms failed in clustered area resulting in a very high number of false alarms. Using the BioSonar however, no detections have been found

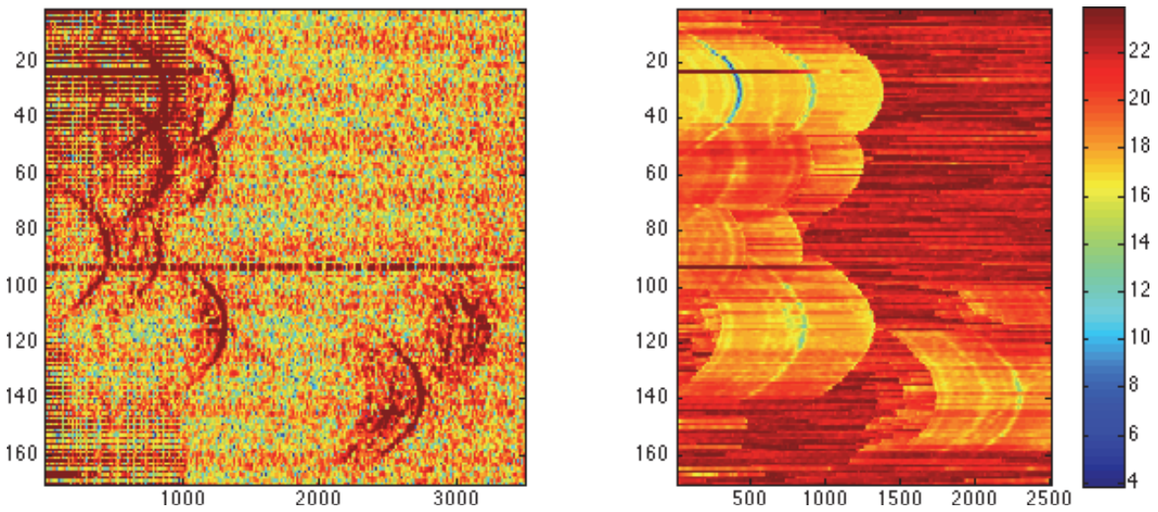

Fig. 10. Left: BioSonar image of the target set. Right: Detection results.

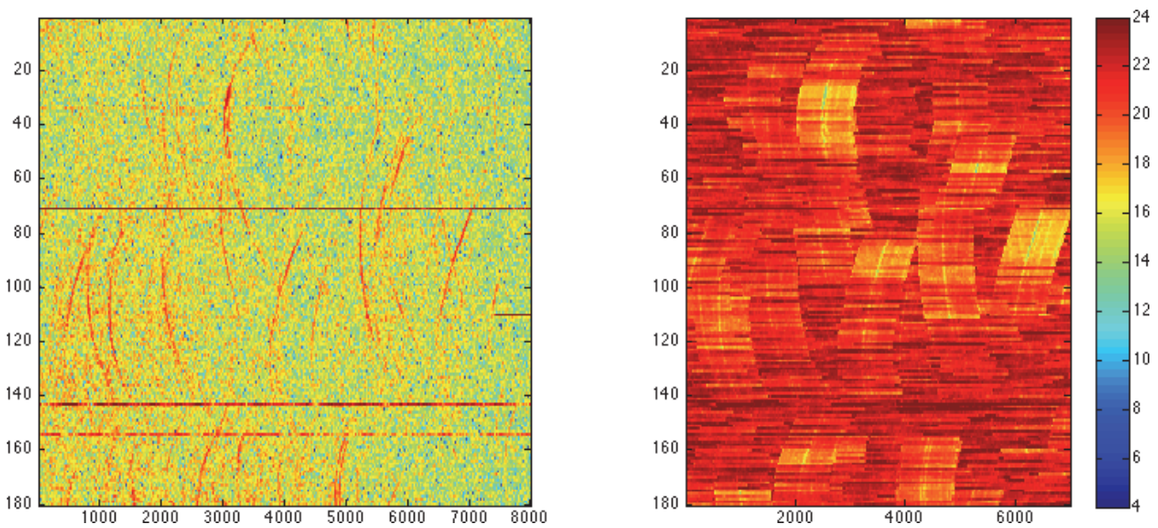

Fig. 11. Left: BioSonar image of the target set. Right: Detection results.

in this area using this algorithm. This demonstrates the potential of the BioSonar system to drastically reduce false alarm rates even with relatively simple and efficient algorithms.

4.2 Cable tracking

Our research group has been running a wideband cable tracking project in parallel with the ongoing work on target detection and recognition. This culminated in a series of trials at Loch Earn in early January 2010, with a demonstration over a 500 m section of cable. An overview of the project and some results from the demonstrations are described in this section.

4.2.1 Background

The targets of interest in this project are US Navy range and communication cables. Samples of various types were provided, varying in external diameter from 32mm down to $16\frac{1}{2}$mm. All of the cable types comprised one or more continuous metallic layers with woven steel

strain wires and a relatively low density plastic sheath. For the final sequence of trials, several substantial sections of a 17mm, polyethylene jacketed cable with a fibre optic core (SL17L) were deployed.

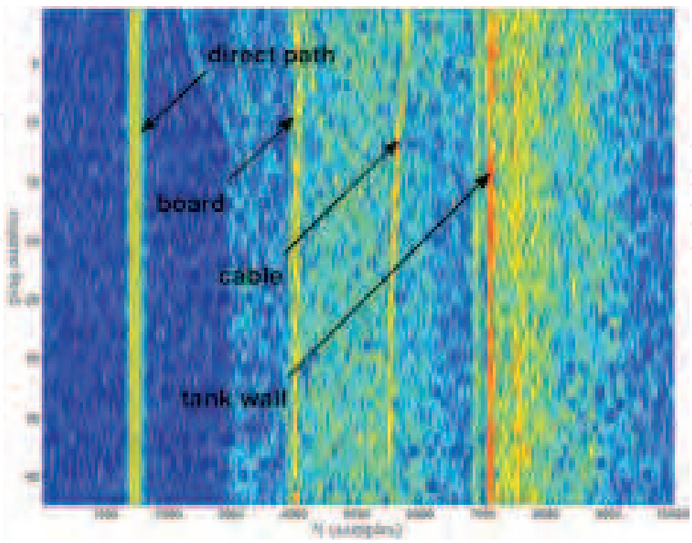

Fig. 12. DC3 echoes at 5 cm intervals along 2 m section of SL17L cable (at 27° grazing angle).

In Brown et al. (2011), the authors demonstrated the detectability of the SL17L cable using the BioSonar in a tank experiment. Figure 12 displays the match filtered echo of a section of SL17L cable lying on soft sediment (sand). The data were recorded using the DC3 bio-mimetic pulse. The cable is clearly visible at the centre of the image. In figure 13 a waterfall plot of the cable echo is shown. Despite the small diameter of the cable, the echo spectra shows strong consistency along its full length, even if a more reliable detector should be built by integrating over sequences of returns.

For the real scale experiment, the BioSonar has been used in a side-looking configuration primarily to facilitate co-operation with the Marine Sonics sidescan unit. The transducer configuration comprises port and starboard projectors and receivers set at a depression angle of 25°.

The detector module operates on single wideband pings and port and starboard channels are treated independently. Visually the cable shows up clearly in imagery produced from the BioSonar system. However, with no hardware time-varying gain (TVG) correction, the background reverberation varies markedly over the sonar swath and simple thresholding cannot be applied. Rather than implement a software TVG, we downsample the data to reduce computational overheads and then estimate local reverberation statistics by fitting a Rayleigh distribution function to the backscatter intensity data. The Rayleigh is a simple, single parameter distribution well suited to modelling sonar intensity data, see Eq.6. Detection follows from the calculation of probabilities or likelihoods that a particular measured pixel value belongs to the estimated distribution. Low likelihoods indicate points that are not well represented by the seabed model and are therefore probable contacts.

$$p(\text{seabed}) = \frac{x}{s^2} \exp\left(\frac{-x^2}{2s^2}\right) \qquad (6)$$
$$p(\text{D}) = 1 - p(\text{seabed})$$

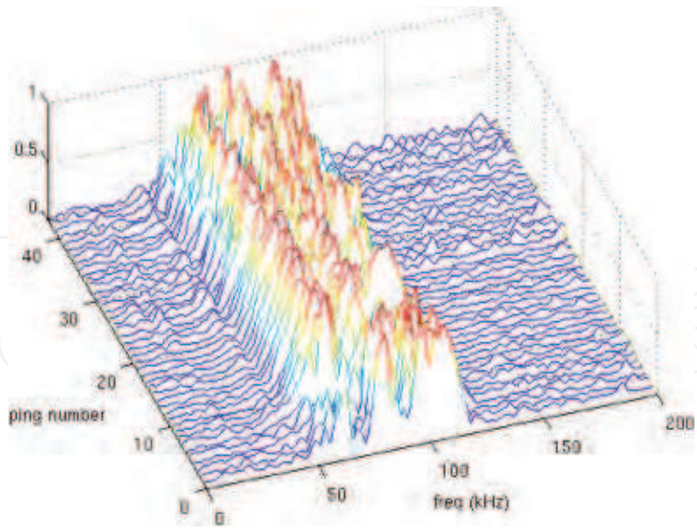

Fig. 13. Waterfall plot of the cable echo spectra whilst the general three-lobed pattern distinctive for this cable/pulse combination is strongly in evidence, variations would make discrimination from a single ping highly difficult and a more reliable detector will be built by integrating over sequences of returns.

For cable detection, running near parallel to the cable, this method benefits greatly from the wide beamwidth of the sonar. Returns are integrated over the full beamwidth, so that contributions are significantly enhanced for a long cable section compared to a more compact target. In this way the $p(\mathrm{D})/p(\mathrm{FA})$ ratio is maximized and a relatively simple detection algorithm can be employed. This is an important consideration given the large quantities of data collected at high data rates and consequent lengthy processing times. At the detector level, thresholds have been set relatively high to ensure the system is not flooded with false alarms. The detections are therefore a little sparser than one would like visually, but provide plenty of information for the tracker to infill where a few pings are missed.

4.2.2 Sidescan and BioSonar sensor comparison

The sidescan and BioSonar sensors perform well in combination, often providing complementary information, and the best tracking results were obtained using the sensors together. For direct comparison, it is possible to generate imagery from the matched filtered wideband data that are similar to conventional sidescan images. These are useful for testing and visualisation, but we should note that they are not fully representative of the quality of the data generated by the sensor and that the wideband detector module is always fed the raw sensor data.

Figure 14 shows a section of sidescan sonar and a corresponding image produced from the BioSonar data. A section of cable is clearly visible on the port side in both sensors. The range is 20m for the sidescan, giving a total swath width of 40m and nearly twice this for the BioSonar.

Figure 15 gives further samples of collocated sidescan and BioSonar data. The cable is clearly visible in the starboard channel for both sensors. When the cable deviates sharply bringing it closer to the vehicle, it is more difficult to track in the sidescan, because of the severe beam pattern characteristic of the MarineSonic sensor. Consequently, the sidescan detector performance is poor in the beam pattern region of the image. Given that a very high frequency

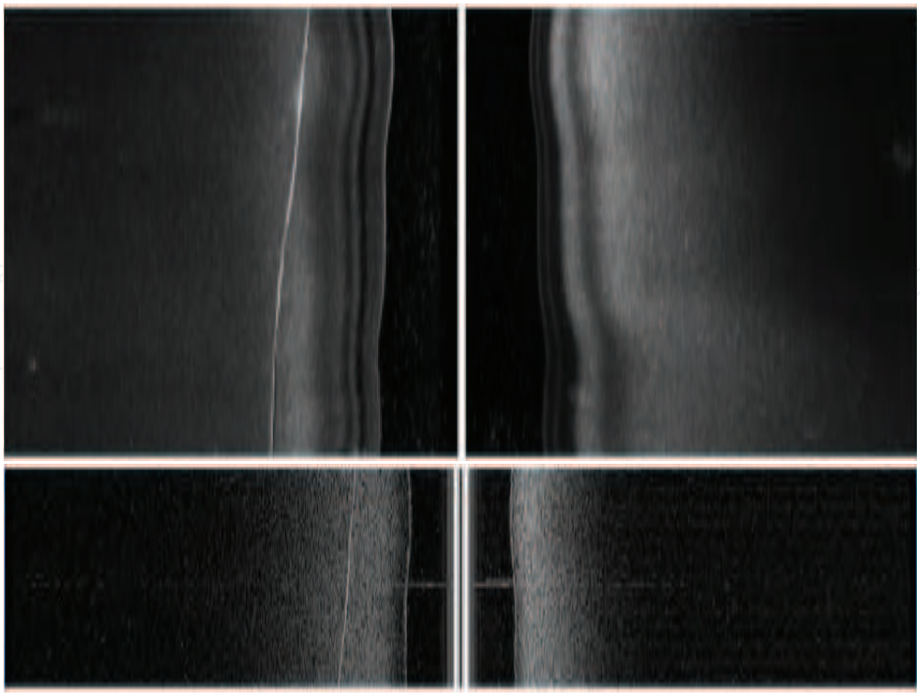

Fig. 14. Top: SS image showing cable in port channel. Bottom: BioSonar image of approximately half the duration with cable in port channel. Note the total swath width is 40m for the sidescan sensor is 75m for the BioSonar.

is required to generate the resolution required for detection in the imagery, this limits the effective channel for tracking to approximately 10m. Here, the BioSonar has two inherent advantages. Firstly, the wide frequency band effectively smooths out frequency dependent nulls in the beam pattern giving a much smoother beam profile and the potential to make continuous detections even when the cable passes beneath the vehicle. Secondly, the lower frequencies available propagate far more effectively and we are able to get good detections beyond 25m. Taken together, these mean that the effective channel width for tracking using the BioSonar is in excess of 50m. In other loch tests stable detections at 40-50m range have been noted where the cable is lying near parallel to the vehicle track. At a higher ping rate and with some parameter modification, the downsampled imagery could also provide a suitable input to the SS detector.

A further advantage in using the BioSonar for tracking is the ability to follow the cable through regions of partial and shallow burial. This is again related primarily to the difference in the operating frequencies between the two sonar systems, though the wide beam width of the BioSonar no doubt plays a role too. Figure 16 demonstrates the problem for the sidescan system. Where the cable goes into burial, detections are dropped. Furthermore, in maintaining a sufficient number of cable contacts to ensure robust tracking, a large number of false detections are generated. In the example shown, tracking is still possible due to the effectiveness of the particle filter tracking module used, but only a small increase in bottom clutter would lead to failure.

Both sensors struggle to detect the cable lying at a steep angle to the vehicle track. The wide beamwidth of the BioSonar works in its favour, but this is offset by the higher operating frequency of the MarineSonic system. Detections are increasingly dropped at angles greater

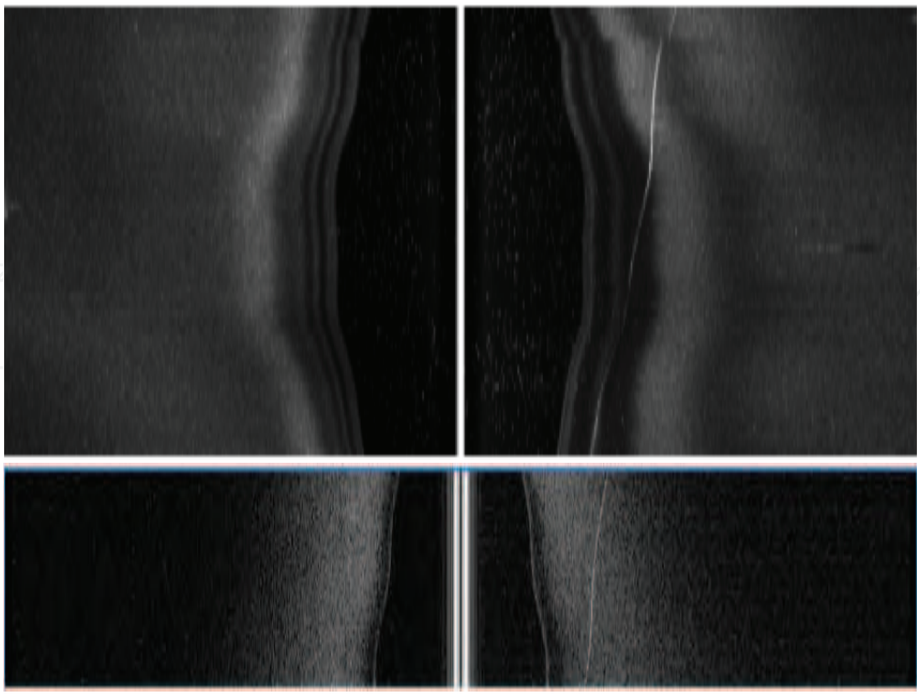

Fig. 15. Top: SS image showing cable in starboard channel. Bottom: BioSonar image of approximately half the duration with cable in starboard channel. The reduced beam pattern effects in the BioSonar data make tracking the cable much easier in these circumstances.

than 20°. The impact of this observation on detections can be seen in Figure 17. This shows cable detections over a c. 300m length of cable. Given the difficulties in deploying the cable using only a small RIB, it was not possible to maintain tensions typical of marine installation. For this reason, the cable has a tendency to follow an elongated spiral trajectory over the loch bed. In places it goes into burial and its direction relative to the vehicle track is subject to large changes. For the BioSonar, burial is not a large problem. The dropped detections are correlated much more clearly with the cable angle. The greatest density of missed detections occurs in the centre of the image, corresponding to some gross vehicle movements, probably initiated by the obstacle avoidance systems. Even here, the remaining sparse detections are sufficient to maintain an active track and on this run a complete unbroken end-to-end survey was completed. The detection rate here is high, but is generated with conservative thresholds so that there are very few false alarms.

The BioSonar system performed well in these trials, but performance could be increased further by more sophisticated detection algorithms. The method chosen here is simple and exceptionally economical. This is essential to be able to process large quantities of wideband data and pass detection packets to the vehicle network for downstream processing given strictly limited computing power in the current BioSonar bottle. The current package was designed for data acquisition only, so the additional computational load provides a severe challenge. It is intended to upgrade the computing power significantly in a future prototype. In addition to improving detector performance, the increased resources will enable full spectral processing of contact segments. We have shown in earlier work that there is sufficient difference in the response of different cable types to provide a positive identification, that is to perform cable recognition. This could be useful, for example, in following a specific cable

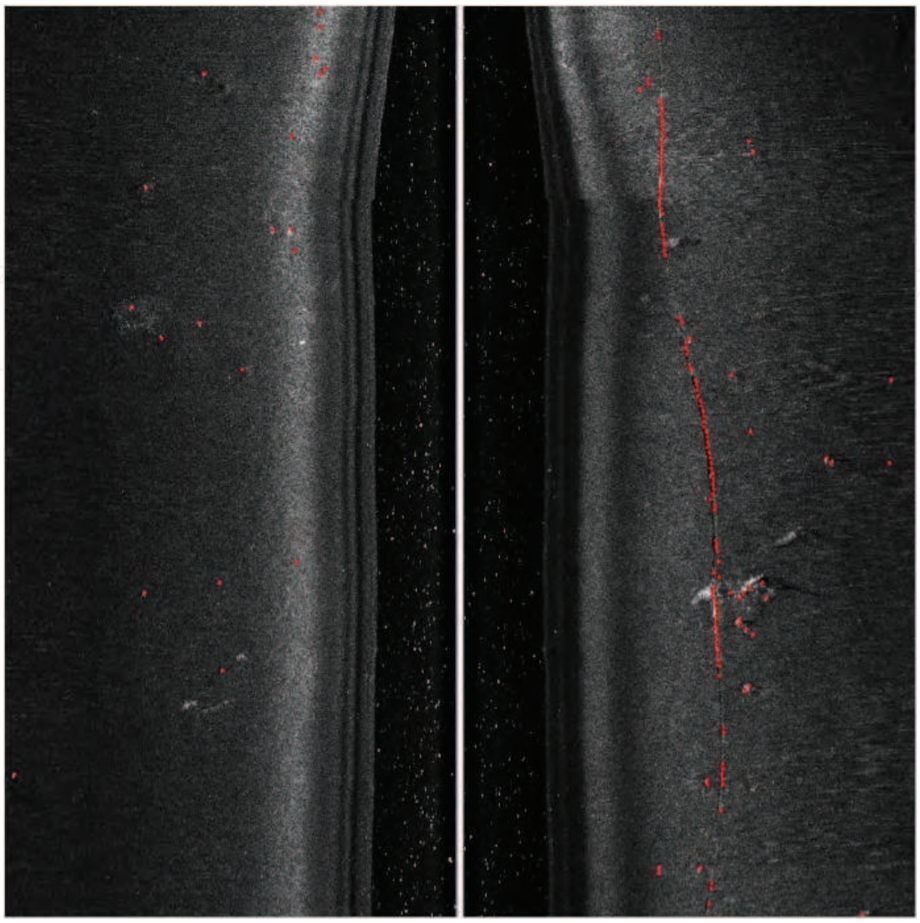

Fig. 16. Sidescan image of the cable lying on the seabed. The red dots are the result of the detection. The sidescan detector fails to detect the cable through regions of partial burial – in these circumstances, generating a sufficient number of cable contacts to maintain a track leads to a large number of false contacts in each image.

through cable crossing regions or in discriminating between cable and other contacts to further drive down the false alarm rate.

5. Conclusion

In this chapter, we described our approach to a bio-mimetic sonar. By answering the question: "what makes the dolphin sonar so efficient?", we created new bio-mimetic broadband pulses. We show that by focusing the energy on different part of the spectrum, these bio-mimetic pulses will react differently depending on the target. By analysing the interaction between sound and objects, we identify stable features based the target resonances. We show how these features can be used for identification purposes. The BioSonar prototype has been built according to the dolphin's sonar characteristics. Because the bandwidth is lower than classical imagery sonars and because its wide beamwidth, the BioSonar losses resolution compared to other sonars. But this resolution loss is compensated by the additional information provided by analysing the echo itself. We demonstrated the capabilities of such sensor in real environment for two particular applications: mine countermeasures and cable tracking.

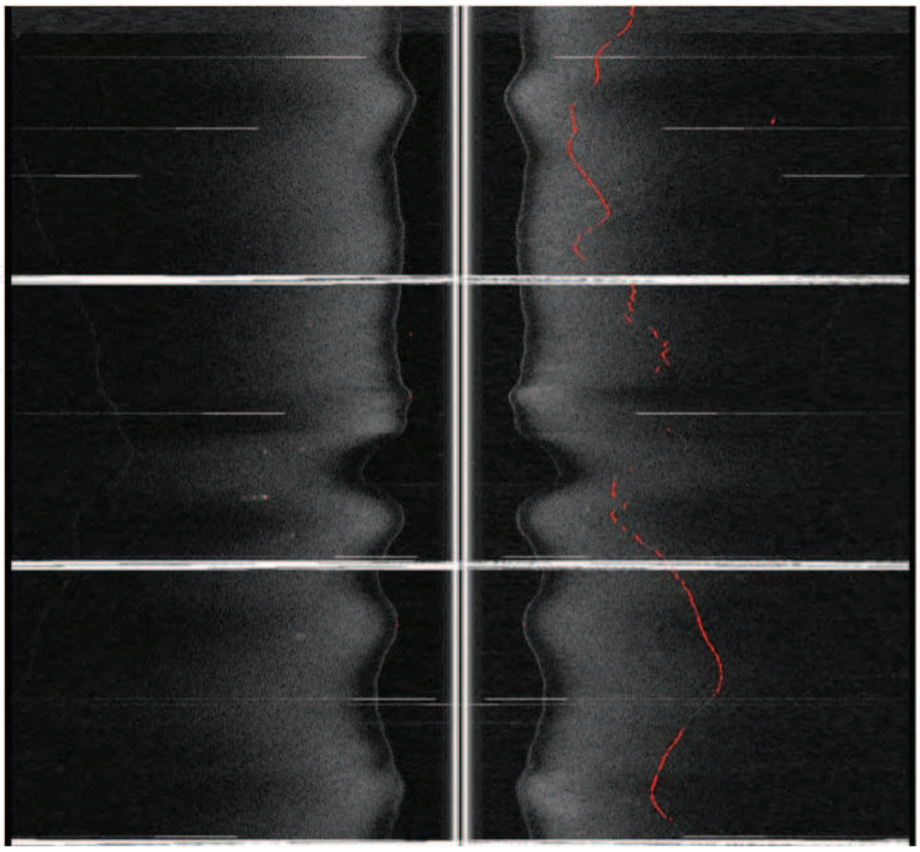

Fig. 17. Approximately 50m section of cable showing the BioSonar detections – the cable is detected through regions of shallow burial. There are very few false contacts and this $p(\mathrm{D})/p(\mathrm{FA})$ ratio is sufficient to maintain a continuous unbroken track for the cable survey.

6. References

Au, W. (1993). *The Sonar of Dolphins*, Springer-Verlag.

Azimi-Sadjadi, M., Jamshidi, A. & Dobeck, G. (2001). Adaptive underwater target classification with multi-aspect decision feedback, Presented at CAD/CAC Conf., Halifax, Novia Scotia, Canada.

Brown, K., Capus, C., Pailhas, Y., Petillot, Y. & Lane, D. (2011). The application of bioinspired sonar to cable tracking on the seafloor, *EURASIP Journal on Advances in Signal Processing* 2011.

Bultan, A. (1999). A four-parameter atomic decomposition of chirplets, *IEEE Trans. Signal Process.* 47: 731–745.

Calder, B., Linnett, L. & Carmichael, D. (1997). Spatial stochastic models for seabed object detection, *Proc. SPIE-Int Soc. Opt. Eng.* 3079.

Calder, B., Linnett, L. & Carmichael, D. (1998). Bayesian approach to object detection in sidescan sonar, *IEE Proc-Vis. Image Signal Proc.* 45(3).

Capus, C. & Brown, K. (2003). Short-time fractional fourier methods for the time-frequency representation of chirp signals, *J. Acoust. Soc. Am.* 113(6): 3253–3263.

Capus, C., Pailhas, Y., Brown, K., Lane, D., Moore, P. & Houser, D. (2007). Bio-inspired wideband sonar signals based on observations of the bottlenose dolphin (tursiops truncatus), *J. Acoust. Soc. Am.* 121(1): 594–604.

Ciany, C. & Huang, J. (2000). Computer aided detection/computer aided classification and data fusion algorithms for automated detection and classification of underwater mines, *Proc. MTS/IEEE Oceans Conf. and Exhibition* 1: 277–284.

Cohen, L. (1995). *Time-Frequency Analysis*, Prentice-Hall.

Dobeck, G., Hyland, J. & Smedley, L. (1997). Automated detection/classification of sea mines in sonar imagery, *Proc. SPIE-Int. Soc. Optics* 3079: 90–110.

Doolittle, R. & Uberall, H. (1966). Sound scattering by elastic cylindrical shells, *J. Acoust. Soc. Am.* 39(2): 272–275.

Dura, E., Bell, J. & Lane, D. (2002). Superellipse fitting for the classification of mine-like shapes in side-scan sonar images, *Proc. MTS/IEEE Oceans Conf. and Exibition*, pp. 23–28.

Faran, J. J. (1951). Sound scattering by solid cylinders and spheres, *J. Acoust. Soc. Am.* 23: 405–418.

Fawcett, J. (2001). Image-based classification of side-scan sonar detections, CAD/CAC Conf., Halifax, Novia Scotia, Canada.

Gaunaurd, G. & Uberall, H. (1983). RST analysis of monostatic and bistatic acoustic echoes from an elastic sphere, *J. Acoust. Soc. Am.* 73(1): 1–12.

Goldman, A. & Cohen, I. (2004). Anomaly subspace detection based on a multi-scale markov random field model, *Signal Processing* .

Goodman, R. & Stern, R. (1962). Reflection and transmission of sound by elastic spherical shells, *J. Acoust. Soc. Am.* 34(3): 338–344.

Hickling, R. (1962). Analysis of echoes from a solid elastic sphere in water, *J. Acoust. Soc. Am.* 34: 1582–1592.

Houser, D., Helweg, D. & Moore, P. (1999). Classification of dolphin echolocation clicks by energy and frequency distributions, *J. Acoust. Soc. Am.* 16: 1576–1585.

Houser, D., Martin, S., Bauer, E., Phillips, M., Herrin, T., Cross, M., Vidal, A. & Moore, P. (2005). Echolocation characteristics of free-swimming bottlenose dolphins during object detection and identification, *J. Acoust. Soc. Am.* 117: 2308Ð2317.

Martin, S., Phillips, M., Bauer, E., Moore, P. & Houser, D. (2003). Application of the biosonar measurement tool, *Proc. MTS/IEEE OCEANS 2003*, p. 311Ð315.

Maussang, F., Hetet, A. & Amate, M. (2007). Higher-order statistics for the detection of small objects in a noisy background application on sonar imaging, *EURASIP Journal on Applied Signal Processing* .

Mignotte, M., Collet, C., Perez, P. & Bouthemy, P. (2000). Hybrid genetic optimization and statistical model-based approach for the classification of shadow shapes in sonar imagery, *IEEE Trans. Pattern Anal. Machine Intell.* 22(2): 129–141.

Moore, P., Roitblat, H., Penner, R. & Nachtigall, P. (1991). Recognizing successive dolphin echoes with an integrator gateway network, *Neural Networks* 4: 701–709.

Pailhas, Y., Capus, C., Brown, K. & Moore, P. (2010). Analysis and classification of broadband echoes using bio-inspired dolphin pulses, *J. Acoust. Soc. Am.* 127(6): 3809–3820.

Perry, S. & Guan, L. (2001). Detection of small man-made objects in multiple range sector scan imagery using neural networks, Presented at CAD/CAC Conf., Halifax, Novia Scotia, Canada.

Petillot, Y., Pailhas, Y., Capus, C., Sawas, J. & Valerie, N. (2010). Target recognition in synthetic aperture and high resolution side-scan sonar, *European Conference on Underwater Acoustics, ECUA 10, Istanbul, Turkey* .

Reed, S., Petillot, Y. & Bell, J. (2003a). An automated approach to the detection and extraction of mine features in sidescan sonar, *IEEE Journal Oceanic Eng.* 28(1): 90–105.

Reed, S., Petillot, Y. & Bell, J. (2003b). A model-based approach to the detection and classification of mines in sidescan sonar, MREP '03 Conf., NATO Saclant Centre, La Spezia, Italy.

Zerr, B., Bovio, E. & Stage, B. (2001). Automatic mine classification approach based on AUV manoeuverability and the COTS side scan sonar, *Autonomous Underwater Vehicle and Ocean Modelling Networks: GOATS 2000 Conf. Proc. CP-46*, NATO Saclant Undersea Research Centre, pp. 315–322.

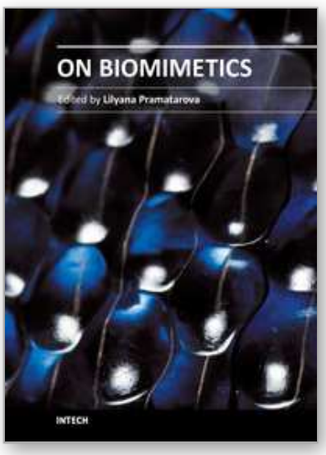

On Biomimetics

Edited by Dr. Lilyana Pramatarova

ISBN 978-953-307-271-5
Hard cover, 642 pages
Publisher InTech
Published online 29, August, 2011
Published in print edition August, 2011

Bio-mimicry is fundamental idea â€˜How to mimic the Natureâ€™ by various methodologies as well as new ideas or suggestions on the creation of novel materials and functions. This book comprises seven sections on various perspectives of bio-mimicry in our life; Section 1 gives an overview of modeling of biomimetic materials; Section 2 presents a processing and design of biomaterials; Section 3 presents various aspects of design and application of biomimetic polymers and composites are discussed; Section 4 presents a general characterization of biomaterials; Section 5 proposes new examples for biomimetic systems; Section 6 summarizes chapters, concerning cells behavior through mimicry; Section 7 presents various applications of biomimetic materials are presented. Aimed at physicists, chemists and biologists interested in biomineralization, biochemistry, kinetics, solution chemistry. This book is also relevant to engineers and doctors interested in research and construction of biomimetic systems.

How to reference

In order to correctly reference this scholarly work, feel free to copy and paste the following:

Yan Pailhas, Chris Capus, Keith Brown and Yvan Petillot (2011). BioSonar: a Bio-Mimetic Approach to Sonar Systems Concepts and Applications, On Biomimetics, Dr. Lilyana Pramatarova (Ed.), ISBN: 978-953-307-271-5, InTech, Available from: http://www.intechopen.com/books/on-biomimetics/biosonar-a-bio-mimetic-approach-to-sonar-systems-concepts-and-applications

INTECH
open science | open minds

InTech Europe
University Campus STeP Ri
Slavka Krautzeka 83/A
51000 Rijeka, Croatia
Phone: +385 (51) 770 447
Fax: +385 (51) 686 166
www.intechopen.com

InTech China
Unit 405, Office Block, Hotel Equatorial Shanghai
No.65, Yan An Road (West), Shanghai, 200040, China
中国上海市延安西路65号上海国际贵都大饭店办公楼405单元
Phone: +86-21-62489820
Fax: +86-21-62489821

IntechOpen